Northern Hemisphere Stratospheric Temperature Response to External Forcing in Decadal Climate Simulations

Abdullah A. Fahad[1,5], Andrea Molod[1], Krzysztof Wargan[1,6], Dimitris Menemenlis[2], Patrick Heimbach[3], Atanas Trayanov[1,6], Ehud Strobach[4], and Lawrence Coy[1,6]

[1]Global Modeling and Assimilation Office, NASA Goddard Space Flight Center, 8800 Greenbelt Rd, Greenbelt, 20771, MD, USA
[2]Jet Propulsion Laboratory, California Institute of Technology, 4800 Oak Grove Dr, Pasadena, 91109, CA, USA
[3]Jackson School of Geosciences, University of Texas at Austin, 2305 Speedway Stop C1160, Austin, TX, US
[4]Agricultural Research Organization, Rishon LeTsiyon, Israel
[5]ESSIC, University of Maryland, 5825 University Research Ct suite 4001, College Park, 20740, MD, US
[6]Science Systems and Applications, Inc., 10210 Greenbelt Rd., Suite 600, Lanham, 20706, MD

Correspondence: Abdullah A. Fahad (a.fahad@nasa.gov)

Abstract. To predict the future state of the Earth system on multiyear timescales, it is crucial to understand the response to changing external radiative forcing (CO_2 and Ozone). Analyzing the Northern Hemisphere (NH) winter stratospheric polar vortex temperature, we found a general temperature decrease in the reanalysis data (1982–2020), the expected trend with increasing CO_2, except for a sharp warming during the period 1992–2000. Results from 1°GEOS-MITgcm coupled general circulation model simulations of past decades show a similar increase in the NH polar stratospheric temperature during 1992–2000 and a decrease during 2000–2020. To isolate the influence of external forcing, we conducted a series of 30-year-long "perpetual" time-slice experiments in which the external forcing for a particular year is held fixed at its values for 1992, 2000, and 2020. Each simulated year of these perpetual experiments is forced with the CO_2, Ozone, anthropogenic aerosol emissions, and trace gases of that year, but none of the simulations include any explosive volcanic forcing. The increasing and then decreasing temperature trend is also manifest in the CMIP6 historical simulations performed with models that include a well-resolved stratosphere. The configuration of the perpetual experiments rules out a direct response to volcanic emissions or a change in the phase of decadal modes of variability as explanations for the warming rather than the expected cooling behavior. Analysis of the temperature budget showed (only significant terms are discussed) that the polar stratospheric temperature behavior is dictated by meridional eddy transport of heat resulting from changes in CO_2 and Ozone over the past decades.

1 Introduction

Seasonal to decadal climate prediction is a relatively new frontier, and accurate prediction relies on the ability of the models to estimate the proper initial state, the proper internal variability, and the proper response to the natural and anthropogenic external forcing (Smith et al., 2007; Keenlyside et al., 2008; Pohlmann et al., 2009; Kirtman et al., 2013; Meehl et al., 2014; Marotzke et al., 2016; Santer et al., 2023). The strong reliance of forecasts at multiyear time scales on both internal variability and the response to changes in external forcing provides a particular challenge for prediction at these long lead times. The ability to

understand and predict how the external forcing, such as changing concentrations of CO_2 and ozone in the atmosphere, drives the climate, as well as how the internal variability on multiyear timescales drives the climate, are both critical for multiyear climate prediction.

Given the established connection between the northern hemisphere (NH) surface weather and climate and the circulation and temperature of the NH lower stratosphere (Thompson et al., 2002; Waugh et al., 2017; Kolstad et al., 2010; Norton, 2003), improving the understanding of the influence of observed levels of external forcing in that region will contribute to the understanding and possible improvement of seasonal to decadal climate prediction skill. For example, the lower stratosphere polar vortex in the NH winter can influence the troposphere and near-surface extreme weather and climate (Thompson et al., 2002; Waugh et al., 2017; Kolstad et al., 2010; Norton, 2003). Analyzing 51 years of reanalyses data and coupled climate models, Kolstad et al. (2010) found that the lower stratosphere polar vortex and temperature associated with it influences the cold air outbreaks in the NH high-latitude regions. Thompson et al. (2002) found a significant relationship between the polar vortex and surface extreme cold events in the NH mid-high latitudes. They concluded that a high level of prediction skill of NH surface cold events can be achieved by predicting lower stratospheric vortex circulation and temperature. The future evolution of Arctic stratospheric ozone also critically depends on the long-term behavior of lower-stratospheric temperatures under increasing concentrations of greenhouse gases and declining ODSs, although there is currently little agreement on the details of the effects of climate change on the Arctic stratospheric polar vortex and polar ozone depletion (Rex et al., 2004; Rieder and Polvani, 2013; Rieder et al., 2014; von der Gathen et al., 2021). The current study enhances understanding of multiyear variability by analyzing the impacts of CO_2 and ozone on Northern Hemisphere climate dynamics using a General Circulation Model (GCM). It offers insights into external forcing influences on multi-year climate, which is crucial for improving future climate prediction accuracy.

Theory and previous studies have shown that with increased CO_2 levels in the atmosphere the global mean surface temperature increases, whereas the stratospheric temperature decreases (Manabe and Wetherald, 1967; Fels et al., 1980; Ramaswamy et al., 2001; Austin et al., 2003; Eyring et al., 2007; Randel et al., 2009; Gillett et al., 2003; Rind et al., 1992, 1998; Manzini et al., 2014; Santer et al., 2023). Using a 40-level General Circulation Model (GCM), Fels et al. (1980) conducted sensitivity experiments with increased levels of CO_2 and/or ozone reduction in the atmosphere and found the stratospheric temperature to decrease due to both perturbations. A uniformly doubled CO_2 in the atmosphere was found to reduce the temperature from the tropopause to approximately 50km uniformly over all latitudes. Rind et al. (1992, 1998) used sets of climate sensitivity experiments with doubled CO_2 levels and found similar results.

Using observed satellite, in-situ, and reanalyses data, Ramaswamy et al. (2001) found significant stratospheric cooling during 1960-1990, including at the NH pole. The study concluded that the observed cooling trend in the stratospheric temperature is due to the radiation change resulting from the depletion of lower stratospheric ozone and to a lesser extent from changes in well-mixed greenhouse gases. However, they also found that a large interannual variability exists in this region from the winter to the spring season. Randel et al. (2009) used updated satellite, radiosonde, and lidar observations from 1979-2007 and found a mean cooling of between 0.5 K/decade and 1.5 K/decade in the stratosphere, with the greatest cooling in the upper stratosphere. The stratospheric temperature anomalies, however, remained constant without any significant trend from the year 1995 to 2005.

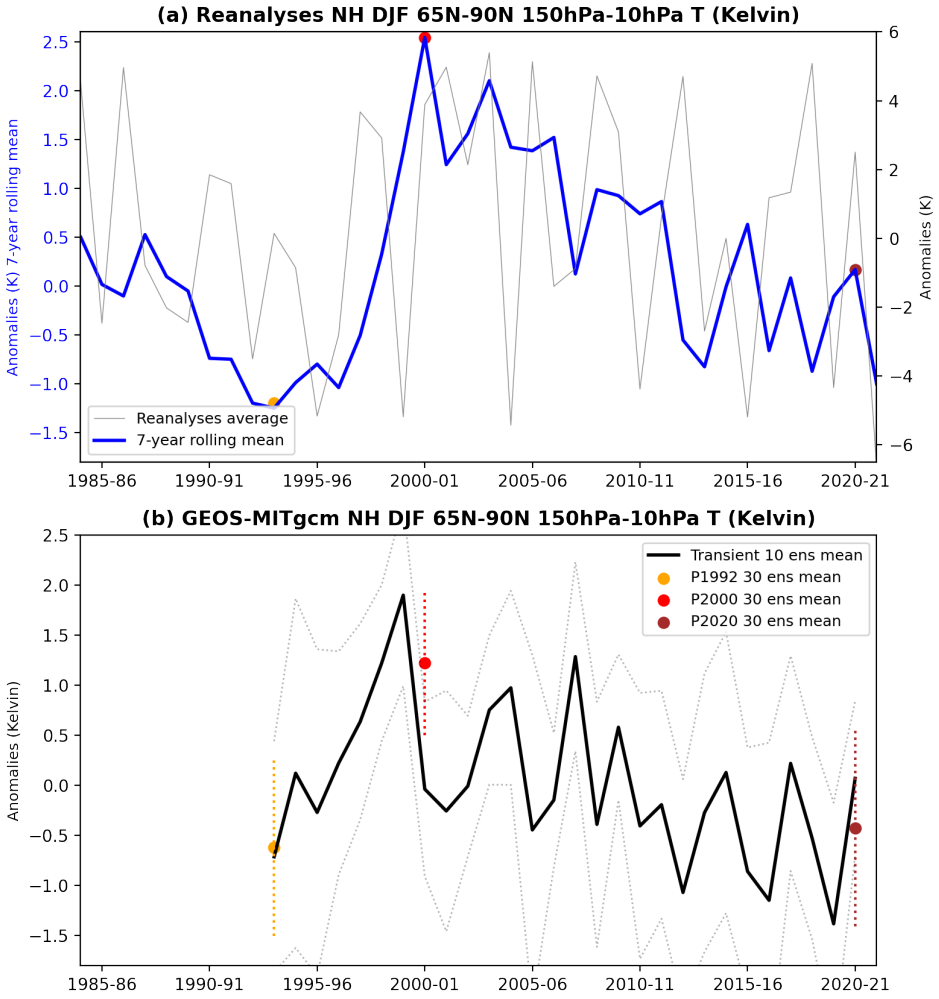

Figure 1. NH DJF mean 150hPa-10hPa and 65°N-90°N mean air temperature anomalies for (a) Reanalysis (MERRA2 and ERA-5), and (b) GEOS-MITgcm. The DJF mean is shown in thin black line and its 7-year running mean in blue in the panel (a). The GEOS-MITgcm 10-member mean transient simulation shown in (b) with bold black line with 1-std spread (grey dotted lines). The 30-member ensemble mean of perpetual experiments is shown in (b) for P1992 (orange line), P2000 (red line), and P2020 (brown line). The 1-std spread of the ensemble is shown with dotted lines. Anomalies are based on 1982-2020 for reanalysis and 1992-2020 for GEOS-MITgcm.

The study assumed that this absence of any statistical trend was due to the high level of natural (dynamical) variability that is present in the NH polar region. Randel et al. (2016) used observations from the series of Stratospheric Sounding Unit sensors to estimate linear trends in stratospheric temperatures between 1979 and 2015. They found a cooling trend, increasing with altitude between the lower the middle, and upper stratosphere (from approximately -0.1 K to -0.5 K per decade). This trend was found to be larger in the first half of the record (1979-1997) than in the following decades. These findings are broadly consistent with the results obtained by Seidel et al. (2016). Polar stratospheric temperature is closely related to the strength

of the mean stratospheric overturning circulation (the Brewer-Dobson Circulation: BDC) with the intensity of air subsidence over the high latitudes in winter being the main 'control knob' for temperature via adiabatic heating. Climate models project an overall acceleration of the BDC with increasing greenhouse gas concentrations (Butchart, 2014; Abalos et al., 2021, and references therein). However, this simple picture is complicated by inter-hemispheric asymmetries in the BDC trends (Stiller et al., 2012, 2017; Ploeger and Garny, 2022) and, more broadly, by differential structural evolution of various aspects of the BDC (Bönisch et al., 2011; Garfinkel et al., 2017; Oberländer-Hayn et al., 2016). Additional complexity arises from the impacts of ozone recovery on the BDC (Abalos et al., 2019; Polvani et al., 2018). The latter two studies demonstrate that the impact of ozone depletion (up to approximately the year 2000) and subsequent recovery outweigh those of the gradual increase in CO2 during the same period, leading to a pattern of acceleration and deceleration of the BDC over the southern polar region during the austral summer. Those studies, however, did not find a similar trend in the northern polar cap temperatures. The study of Zhou et al. (2019) demonstrates a nonlinear response of the NH polar vortex temperature to the tropical western Pacific heating associated with SST change during DJF. The study showed that increasing levels of heating over the western tropical Pacific excite stationary Rossby-type waves that propagate to the NH high-latitude upper troposphere, and impact the temperature of the polar vortex in a non-linear fashion. However, the details of the pathway by which the tropical diabatic heating forces the NH polar vortex still remain unexplored.

Analyzing reanalysis data, we found NH polar vortex temperature decreases in the satellite record (1982–2024) during winter; however, a sharp warming period exists from 1992 to 2000 (Fig. 1a). This warming trend is opposite to what we expect from a response to a CO_2 increase in the atmosphere. The present study aims to explore NH winter polar stratospheric temperature change in recent decades using GEOS-MITgcm coupled decadal climate simulations. We investigate these processes using ensembles of 'perpetual' time-slice and transient experiments with our GEOS-MITgcm coupled model to understand what drives the initial cooling at the end of the period (1992), the peak of sharp warming (2000), and one of the recent cooling years (2020) (Fig. 1a). Specifically, the study examines this temperature evolution, evaluates the role of external forcing from CO_2 and ozone change, and identifies a dynamical pathway by which this external forcing impacts the NH polar stratospheric temperature. Section 2 of this study describes the model, the experimental design, and the reanalyses data that were used in this study. The findings of this study are documented in Section 3. Sections 4 and 5 are the discussion and conclusions of this study based on the results from Section 3.

2 Methodology and Data

Observationally based estimates of meteorological fields were obtained from the Modern-Era Retrospective analysis for Research and Applications, Version 2 (MERRA-2) (Gelaro et al., 2017; GMAO, 2015) and ECMWF Reanalysis 5th Generation (ERA5) (Hersbach et al., 2020) reanalyses for the years 1982-2024. Long-term temperature variability and trends in reanalyses are affected by step changes in the assimilated observations and generally have to be treated with caution. However, a detailed evaluation conducted as part of the Stratosphere-Troposphere Processes And their Role in Climate Reanalysis Intercomparison project (Fujiwara et al., 2022; Long et al., 2017) indicates that these changes affect mainly the upper stratosphere (not con-

sidered here) and occur mainly before 1998. Post-1998 stratospheric temperatures at pressures greater than 10 hPa are robust among the modern reanalyses (Fujiwara et al., 2022).

To understand the NH stratospheric climate response in the past decades, we used the Goddard Earth Observing System-MITgcm (GEOS-MITgcm) coupled earth system model at a nominal 1-degree horizontal resolution in the atmosphere and ocean, with 72 hybrid vertical levels in the atmosphere (top lid 0.01 hPa) and 50 levels in the ocean. Details of the model can be found in (Strobach et al., 2022), but some aspects relevant to this study are described here. The atmospheric model includes the finite volume dynamical core on a cubed sphere grid (Putman and Lin, 2007), a full suite of physical parameterizations including the two-moment cloud microphysics (which includes the aerosol indirect effect) of Barahona et al. (2014), the land model of Koster et al. (2000), and is coupled to the Goddard Chemistry Aerosol Radiation and Transport (GOCART) interactive aerosol model Chin et al. (2002); Colarco et al. (2010). The aerosol emissions in the simulations described here do not include explosive volcanics. The MITgcm has a finite-volume dynamical core (Marshall et al., 1997) with a nonlinear free-surface and real freshwater flux (Adcroft and Campin, 2004). The MITgcm was configured with a 100 km horizontal grid on a "Lat-Lon-Cap" grid (Forget et al., 2015), and 50 vertical levels.

To investigate the NH lower stratospheric temperature change on multiyear time scales, we conducted both an ensemble of transient simulations and 30-year long 'perpetual year' time-slice simulations, for which the external forcing in a particular year is repeated 30 times. The 'perpetual year' simulations are similar in structure to CMIP6 pre-industrial simulations for the long-term ($\sim$500 years) simulation is fixed to 1850 forcing for each year and only driven by internal variability (Eyring et al., 2016). We ran 'perpetual year' simulations corresponding to three different years; the year 1992 (P1992), the year 2000 (P2000), and the year 2020 (P2020), each forced with the respective year's CO_2 and Ozone (O_3). The specific years chosen for these simulations are the inflection points in the NH lower stratospheric temperature time series shown in Figure 1a and indicated by the filled circles. In these 'perpetual' simulations, the annual cycles of CO_2 emissions and ozone are fixed at the perpetual year as the simulation progresses, resulting in a repetition of the same year's external forcing 30 times. The 30 years of simulation are regarded here as a 30-member ensemble of simulations of the 'perpetual' year, as the initial states for each perpetual year are assumed to be uncorrelated. This assumption is consistent with other studies, eg., (Zhou et al., 2024; Alexander et al., 2004; Portal et al., 2022). The external boundary conditions of the 'perpetual' experiments repeat annually while the internal atmospheric state varies, each year of the simulation functions as an independent ensemble member (or realization) of that specific year's climate. The 30-member ensemble mean of these experiments does not realistically simulate the phase of low-frequency modes of internal variability, so the differences among the perpetual experiments are due only to the influence of the differences in external forcing. The annual global mean CO_2 level for P1992 is 356ppm, for P2000 is 368ppm, and for P2020 is 413ppm. There are no explosive volcanic emissions included in any of the perpetual simulations, but the experiments are conducted with prescribed ozone, which is impacted by volcanic emissions (Cionni et al., 2011), and so an indirect impact of volcanic emissions is included in our experiments.

The initial conditions for the 30-year long perpetual experiments are all taken from the same spun-up GEOS-MITgcm state (Year 2000), originally initialized with Modern-Era Retrospective analysis for Research and Applications, Version 2 (MERRA-

2) (Gelaro et al., 2017) (MERRA-2) and Estimating the Circulation and Climate of the Ocean (ECCO) data (Wunsch and Heimbach, 2007; Forget et al., 2015) (ECCO).

The first years of the P1992, P2000, and P2020 perpetual experiments were initialized from a common state and each runs freely with forcings specific to their respective years (with individual years from the perpetual runs acting as ensemble members). This design ensures that low-frequency signals, such as decadal SST modes, evolve into different phases across the ensemble members (details on the phase spread are provided in the Discussion section). Consequently, these modes cancel out in the ensemble mean, effectively removing low-frequency variability as a potential driver of the stratospheric warming event.

The initial conditions for the 10-member ensemble of transient experiments were randomly chosen from the 1992 perpetual experiment. Each year of the transient experiment is forced with observed CO_2 (CMIP, Eyring et al. (2016)), O_3 and aerosol (Randles et al., 2017) emissions (excluding explosive volcanics) from the correct year of the simulation. The low-frequency SST modes are out of phase across these ensemble members, minimizing their influence when computing the ensemble mean (more details are in the Discussion section).

The GEOS-MITgcm coupled model transient simulations reproduce the mean state and variability of the polar vortex reasonably well as compared to reanalyses. The geopotential height at 10 hPa from the 10-member ensemble mean for January over 1992–2020 shows a similar mean state and location of the NH polar vortex during winter compared to reanalysis (MERRA-2: 1992–2020) (Fig. 2 a,b). The 30-year mean January momentum-flux variance ($U'V'$) associated with the vortex wind jet, calculated from sub-monthly fields (these variances are computed as the deviation of the 6-hourly values from the monthly mean), further shows that the stability and variability of the vortex core are simulated reasonably well in the GEOS-MITgcm compared to the reanalysis (Fig. 2 c,d). The model, however, produces a bit weaker mean geopotential height ($\sim$ 4km higher at the core) and momentum flux variance (weaker $\sim$ 25 m^2/s^{-2} near Greenland) compared to MERRA-2, suggesting that the simulated vortex may be a bit more resilient under extreme wave forcing. This could be a result of a lack of higher vertical resolution in the stratosphere. However, the close agreement in both mean height structure and eddy flux confirms that the model faithfully represents the polar vortex's stability and natural variability.

As part of the analysis of results, the diabatic heating is taken directly from the model output as a sum of temperature tendencies due to longwave radiation, shortwave radiation, moist processes, turbulent sensible heating, and gravity wave drag (Molod et al., 2015; Bosilovich, 2015; Fahad et al., 2020). The eddy component of the meridional atmosphere heat transport is calculated following Holton and Hakim (2012) (See Appendix, section 6 for more details). We analyzed the contributions to the meridional heat transport by steady symmetric circulations ($[\overline{V}][\overline{T}]$), stationary eddies ($[\overline{V^*}\ \overline{T^*}]$), and transient eddies ($[\overline{V'T'}]$, see Section 6). Here, T and V are the temperature and meridional components of the wind field, respectively. Square brackets denote the zonal average, and the overbar is the time average (DJF seasonal mean over all years/ensemble member). The corresponding departures from the time and zonal averages are indicated by an asterisk and a prime, respectively.

Winter and springtime polar stratospheric temperature is highly correlated with the strength of air subsidence over the high latitudes, which is, in turn, related to the intensity of wave activity in the extratropics (Shaw and Perlwitz, 2014; Newman et al., 2001). To quantify the strength of the residual circulation, we use the transformed Eulerian mean (TEM) mass stream function calculated as in Birner and Bönisch (2011). The Eliassen Palm (EP) flux is defined following Edmon Jr et al. (1980). The EP

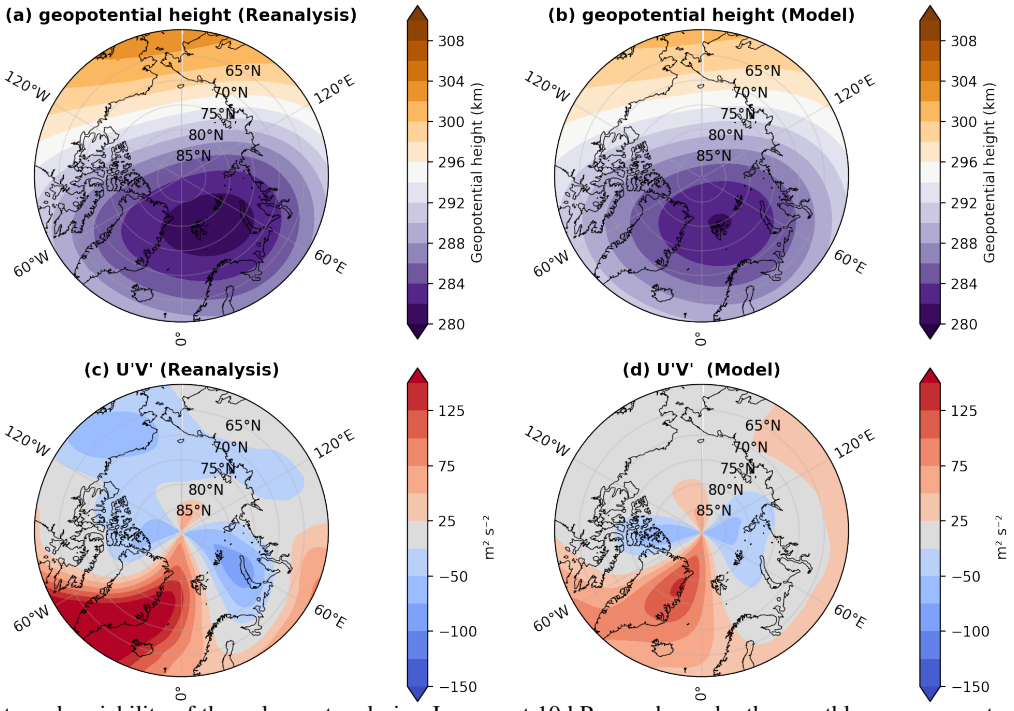

Figure 2. The mean state and variability of the polar vortex during January at 10 hPa are shown by the monthly mean geopotential height (km) and momentum flux (m^2/s^{-2}) (U′V′, calculated from sub-monthly fields) for the MERRA-2 reanalysis (1992–2020) in panels (a) and (b), and for the GEOS-MITgcm 10-member ensemble mean (1992–2020) in panels (c) and (d). The model reproduces a mean state and stability similar to those in the reanalysis.

flux is a two-component vector field that measures the intensity and direction of zonally averaged wave propagation in the meridional plane. Its divergence is closely related to wave-zonal flow interaction strength (Andrews et al., 1987). In particular, convergence (negative divergence) of the EP flux indicates wave dissipation, which decelerates the zonal flow and accelerates mass subsidence at high latitudes. The reverse is true for positive divergence.

To calculate the significance of the difference in means between the ensembles of different experiments, we primarily used a two-sided t-test. Additionally, we performed a nonparametric bootstrap significance test using $\alpha = 0.05$ (95% confidence) and 1,000 bootstrap random samples to assess whether the mean difference between the two datasets was statistically significant without assuming normality. We found similar conclusions for all analyses with the bootstrapping significance test, with results that were slightly more stringent than those from the t-test.

3 Results

3.1 NH Stratosphere Response in Decadal Climate Simulations

Examination of DJF temperatures averaged between 150 hPa and 10 hPa and between 65° N and 90° N from MERRA-2 and ERA5 (Fig. 1a) reveals an overall negative trend over the NH polar vortex from 1982 to 2020, with the exception of a strong warming trend from 1992 to 2000. The DJF mean temperature trend during 1992–2000, although over a short time range, is strong and becomes evident in the 7-year running-mean (the warming trend is insensitive to the window size) time series, which filters out some of the interannual variability (Fig. 1a). This sharp warming from 1992 to 2000 contradicts the general expectation that the stratosphere cools as the sea surface and troposphere warm in response to increased CO_2. It is also the only period in the reanalysis record exhibiting such a pronounced, significant temperature trend.

In this study, we focus on the years 1992 to 2020 to investigate the temperature behavior and compare the end of the initial cooling period (1992), the peak of the transient warming (2000), and the recent resumption of cooling at the end of the time series (2020). The 10-member ensemble mean of the transient GEOS-MITgcm climate simulations from the years 1992-2000 and 2000-2020 (Fig. 1b) shows similar behavior in the NH stratospheric high latitude temperature, with a strong positive temperature trend in the first period of 1992-2000, and a strong cooling temperature trend from 2000 to 2020.

The polar stratospheric temperature behavior found here is consistent with the findings of Fu et al. (2019), who found a positive lower stratospheric temperature trend in the 1990s in both hemispheres winter (especially during September for the Southern Hemisphere), whereas the trend is negative during years 2000 to 2018. Focusing on the Southern Hemisphere, Fu et al. (2019) concluded that this overall temperature trend in September months in the Southern Hemisphere is most likely due to the ozone healing process after the year 2000.

In the transient experiments and reanalysis data, low frequency internal variability might influence the year-to-year changes, and here we wish to isolate the influence of the external forcing. The 30-member ensemble mean of the perpetual experiments will substantially minimize the influence of internal variability, and so any behavior seen in the transient experiment that is replicated in the perpetual experiments can be attributed to external forcing.

Figure 3 shows the zonal mean NH DJF mean air temperature (T) as a function of pressure for the perpetual experiments in the left panels (a, b, and c), and the difference between pairs of perpetual experiments in the right panels (d, e and f). The difference between the 30-member ensemble mean of perpetual experiments P2000-P1992 (Figure 3d) shows that there is a strong warming in the NH stratosphere at high latitudes (65°N-90°N). In contrast, the difference between P2020 and P2000 shows a strong cooling in the NH stratosphere's high latitudes (Fig. 3e). Due to this opposing stratospheric temperature change during the two intervening periods, the difference between P2020 and P1992 shows no significant change in much of the region. The significance tests to calculate 95% confidence were conducted using t-tests and bootstrapping, and yielded similar confidence conclusions for the warming and cooling patterns. The results from the perpetual experiments are consistent with the transient experiment discussed earlier (Fig. 1, & 3). In passing, we note that the stratospheric cooling at midlatitudes is consistent with the expected radiative effects of increasing CO_2 (Manabe and Wetherald, 1967; Ramaswamy et al., 2001).

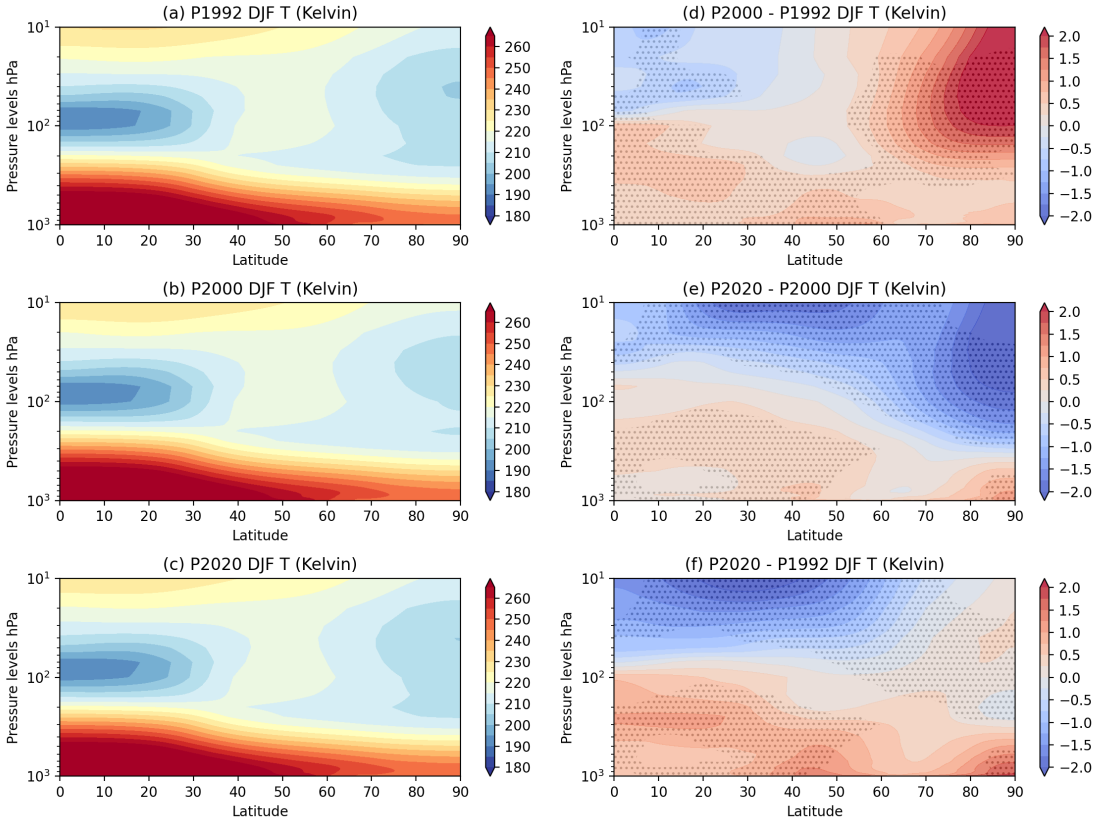

Figure 3. Zonal Mean NH DJF air temperature (T) mean for (a) P1992, (b) P2000, (c) P2020, and (d) difference between P2000 - P1992, (e) difference between P2020 - P2000, (f) difference between P2020 - P1992; (unit: Kelvin). Figures are stippled at 95% significance computed using a difference of means 2-sided t-test from the 30-member ensemble sample.

As discussed in Section 2, trends in reanalyses may be due to changes in the mix of observations used in the assimilation as well as to low-frequency internal variability, and/or to changes in the external forcing. The agreement among our perpetual experiments that used constant CO_2 and ozone levels from specific years, our transient experiments, and reanalyses from the same period suggests that external forcing related to the CO_2 and ozone concentrations in the atmosphere is the key factor responsible for the change in stratospheric temperature trends.

To analyze the proximate cause of the warming and then cooling of the high-latitude stratosphere, the individual temperature tendency terms from the different physical and dynamical model processes were examined. The largest tendency terms are those due to the longwave (there is little solar forcing in boreal winter) and those due to dynamical processes. The longwave tendency in the perpetual experiments shows a negative change in longwave cooling (cooling increases) from the P1992 to P2000, which would tend to cool the atmosphere, and a positive change (cooling decreases) from the P2000 to P2020 in the NH high latitude stratosphere (Figs. 4d & e), which would tend to warm the atmosphere. The behavior during both periods suggests that the

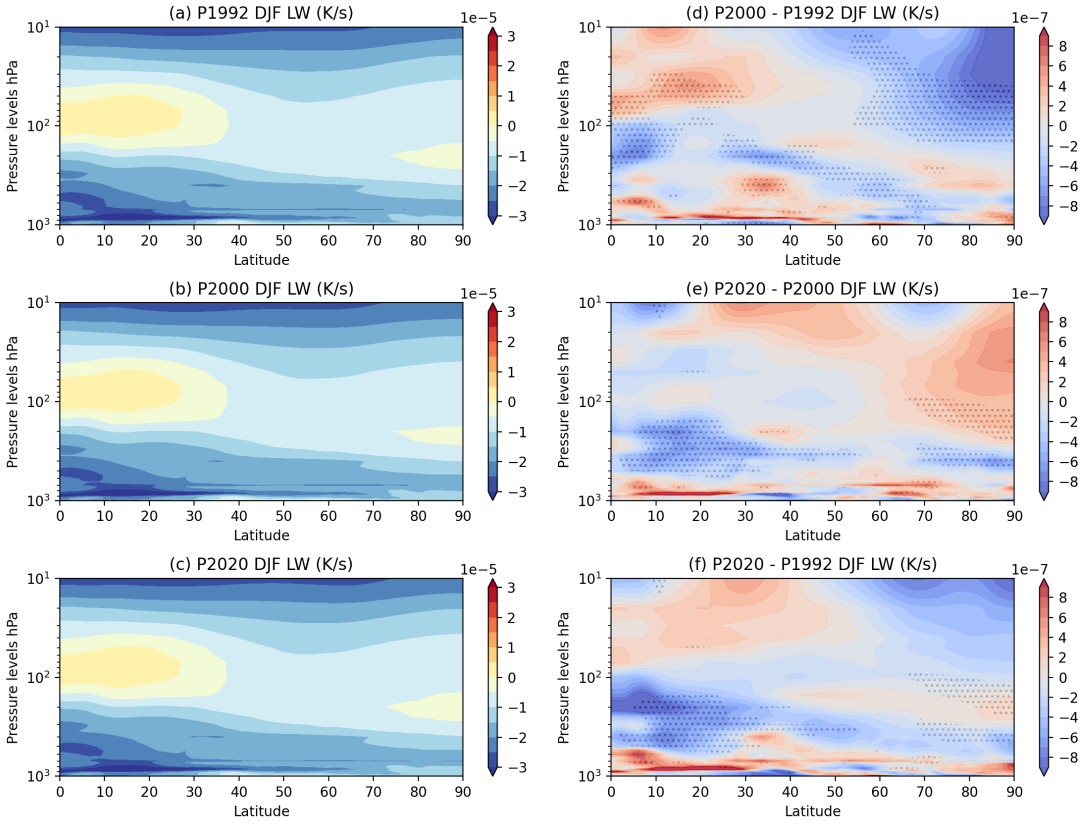

Figure 4. Zonal Mean NH DJF Longwave Cooling mean for (a) P1992, (b) P2000, (c) P2020, and (d) difference between P2000 - P1992, (e) difference between P2020 - P2000, (f) difference between P2020 - P1992. Figures are stippled at 95% significance computed using a difference of means 2-sided t-test from 30-member ensemble sample.

change in the longwave cooling rates are a result of the temperature change, rather than a cause of the change. This leaves the dynamical tendency term as the proximate cause of the temperature change.

3.2 Dynamical Mechanism of Proximate Cause of Heating

The polar cap wintertime temperature at high latitudes is largely driven by the vertical component of the residual circulation in that region on interannual time scales (Newman et al., 2001). In the TEM formulation the variability of the vertical component is determined primarily by the zonal mean horizontal eddy heat flux (alongside the zonal mean vertical velocity) (Shaw and Perlwitz, 2014). To articulate the role of the dynamic tendency terms on the NH stratospheric polar temperature we therefore begin by analyzing the eddy heat flux from the three sets of perpetual-year simulations. The sum of the stationary and transient components of the heat flux is shown in Fig. 5. The meridional eddy heat flux to the NH pole increases from the P1992 to the P2000 simulation, whereas it decreases from the P2000 to the P2020 simulation (Fig. 5). The increased eddy heat flux from the

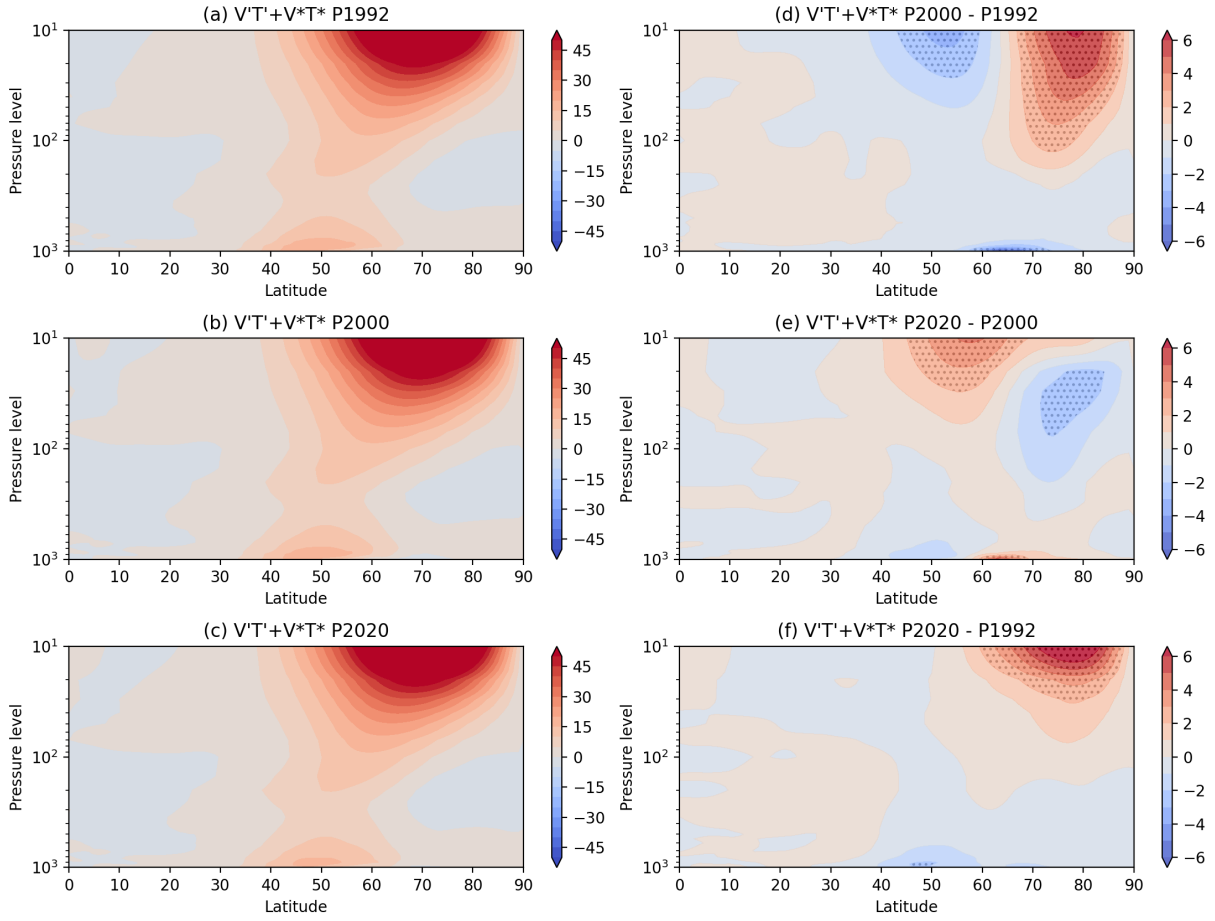

Figure 5. Zonal mean DJF mean V'T' + V*T* in Kms^{-1} for (a) P1992, (b) P2000, (c) P2020, (d) P2000-P1992, (e) P2020-P2000, and (f) P2020-P1992. Figures are stippled at 95% significance computed using a difference of means 2-sided t-test from 30-member ensemble sample.

P1992 to the P2000 experiment is due to both stationary wave (V^*T^*) (Fig. S2d) and transient wave ($V'T'$) (Fig. S3d) activity. The meridional eddy heat flux decrease fro P2000 to P2020 is also due to both the stationary wave (V^*T^*) (Fig. S2e) and the transient wave ($V'T'$) activity decrease (Fig. S3e). The analysis from here onward in the study makes no distinction between the contributions from transient and stationary waves.

Figure 6 shows the residual mass stream function (see equation A2) for the periods of interest and its difference from one period to the other. Evident is an intensification of the residual circulation between 1992 and 2000 (red shading in Fig. 6a), followed by a weakening after 2000 (blue shading in Fig. 6b). In particular, there is an increase (decrease) of air subsidence in DJF over the high latitudes in the early (late) period. This implies a strengthening (weakening) of adiabatic warming in P2000-P1992 (P2020-P2000), and this finding is qualitatively consistent with the pattern of temperature changes in Figures 3 and 1.

We note that the differences in the intensity of subsidence over the pole in Figure 6 are in agreement with the convergence of mean eddy heat flux shown in Figure 5. While the polar temperatures in 2020 approximately return to the 1992 values (Figure 1), the intensity of the streamfunction in 2020 still exceeds that in 1992 (Figure 6).

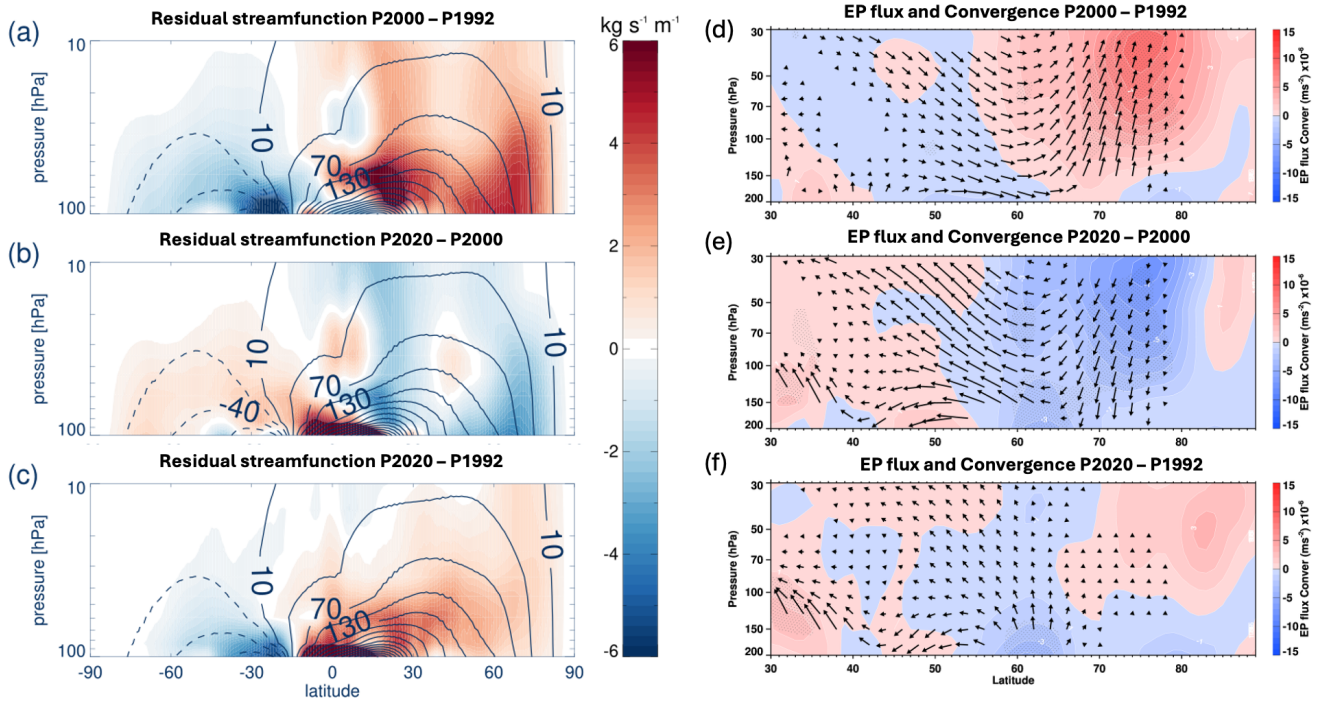

Figure 6. Mean Residual streamfunction (a,b,c), and EP flux with convergence (d,e,f) during DJF from model simulations. Contours: mean residual streamfunction divided by the Earth's radius for 1992 (a and c) and 2000 (b). Shading: the streamfunction change for (a) P2000-P1992, (b) P2020-P2000, and (c) P2020-P1992. EP flux (vector) (unit: m^2/s^2) and convergence (shaded) (unit: m/s^2) for (d) P2000-P1992, (e) P2020-P2000, and (f) P2020-P1992. Convergence is shown in red and divergence is shown in blue. Figures are stippled at 95% significance computed using a difference of means 2-sided t-test from a 30-member ensemble sample.

The stratospheric residual circulation is driven by momentum deposition from Rossby wave breaking interacting with the zonal flow in the midlatitudes (Andrews et al., 1987). This is quantified by the EP flux convergence, wherein positive convergence decelerates the zonal mean zonal wind and induces subsidence over high latitudes. Figure 6 (d,e,&f) shows the changes in the EP flux and its convergence between P2000-P1992, P2020-P2000, and P1992-P2000. The upward-pointing arrows and the increase in convergence at midlatitudes in panel (d) indicate an intensification of wave activity and wave breaking between 1992 and 2000. This is consistent with the strengthening of the residual circulation during that period (Figure 6a) and, consequently, with the increase in polar temperature. The converse is true for the changes between 2000 and 2020. The overall change between 1992 and 2020 (panel f) is also consistent with the intensification of the residual circulation over the same period (Fig. 6c).

4 Discussion: Why the different behavior in different time periods

Our 10-member mean transient external forcing experiments, as well as our perpetual experiments, show opposing NH lower stratosphere temperature trends for the years 1992-2000 and for the years 2000-2020, in agreement with reanalysis data. We have shown that this pattern is directly due to the strengthening and then weakening of the dynamical heating (as opposed to radiative heating), consistent with the strengthening (1992-2000) and subsequent weakening (2000-2020) of the mean meridional circulation due to changes of the Rossby wave activity (both stationary and transient) over these two periods.

The changes in the dynamical heating between these two periods examined here could potentially be associated with low-frequency modes of internal variability, such as the Interdecadal Pacific Oscillation (IPO, (Meehl et al., 2016)), or direct radiative forcing due to explosive volcanics. We argue here that our simulation design and the analysis performed here suggest that the low frequency climate variability and the direct impact of explosive volcanics are not responsible for the NH DJF stratospheric temperature behavior discussed here.

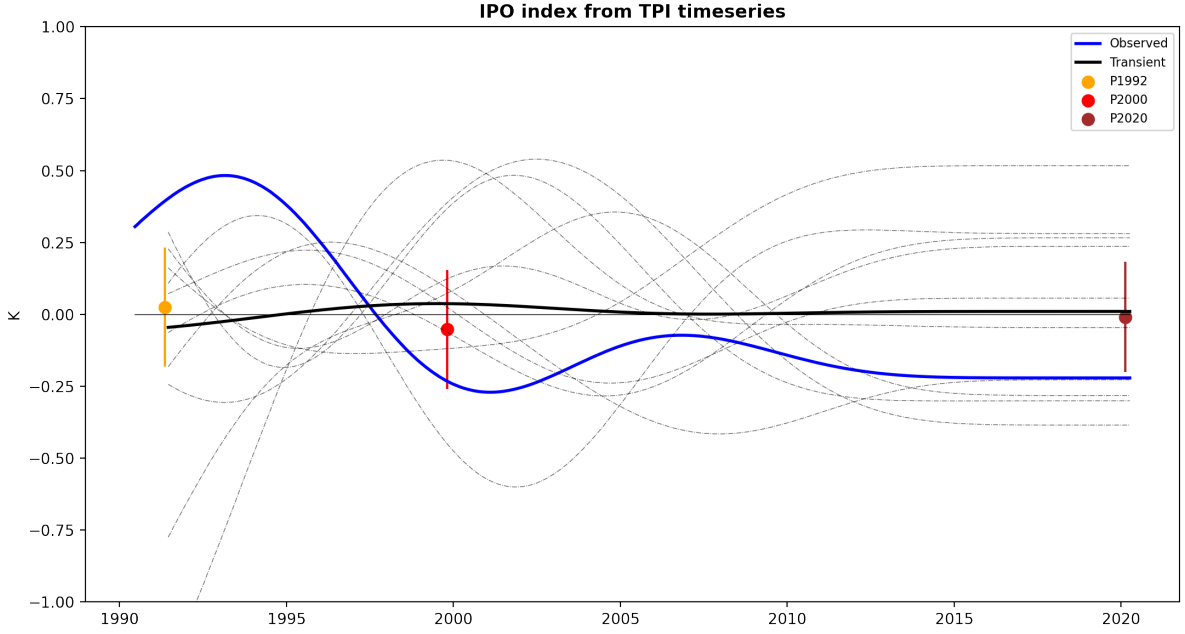

Figure 7. Tripole Index (TPI) for the Interdecadal Pacific Oscillation (IPO) timeseries is shown for observed data (blue line, NOAA OI SST V2) and model simulations. The black line shows the 10-member ensemble mean, while dotted lines show individual simulations. Perpetual experiments are shown with their 1-std spread for P1992 (orange), P2000 (red), and P2020 (brown). Anomalies are calculated based on the 1992-2020 baseline year.

Figure 7 shows that the ensemble mean of 30 ensemble members effectively minimizes any low-frequency variability, despite the individual ensembles starting from different initial states. The P1992, P2000, and P2020 perpetual experiments were initiated from the same initial conditions and were run freely with the forcings specific to their respective years. We

illustrate the dismissal of low-frequency variability as responsible for the NH stratospheric polar temperature behavior with the IPO, as detected using the Tripole Index (TPI). The global mean surface temperature trend is positive during the positive phase of the IPO, and negative during the negative phase. The observed TPI is shown as the blue line in Figure 7. The transient experiment ensemble members TPI are shown in the dashed lines, and the transient experiment ensemble mean is shown with the solid black line. The influence of the IPO in the transient experiment ensemble mean is essentially removed, so the behavior of the ensemble mean stratospheric temperature in the ensemble mean of the transient experiments cannot be due to the IPO. Similar arguments can be made about other low-frequency modes of variability. In addition, the ensemble mean TPI from the perpetual experiments, shown by the yellow, orange, and brown dots in the figure, also shows a damped mean IPO signal. Experiments analyzed in detail here are a 30-member ensemble mean of 'perpetual year' experiments, so the contribution to our results from low-frequency modes such as IPO is negligible. The widespread of IPO phases and the damping of the IPO in the ensemble mean is due in part to our sampling of spun-up initial conditions, and due in part to the model's fidelity in capturing the correct phase of the IPO. The inability of ensembles of free-running models to capture the IPO is consistent with the findings of Meehl et al. (2014), who determined that only a handful of CMIP ensembles (randomly) whose IPO phases matched observations could successfully reproduce the observed global mean surface temperature trend (Meehl et al., 2014).

The influence of direct volcanic emission on the temperature trends being discussed in this study can be dismissed based on our experiment design. In our experiments, the spun-up initial state's aerosol field does not contain aerosols emitted from Pinatubo (Supplementary Fig. S4), and explosive volcanic emissions are not included in the emissions that drive the interactive aerosol model.

One further mechanism that can influence the changes in the meridional heat flux is an indirect affect of volcanic emissions through the impact on the ozone. It is plausible that the 1991 eruption of Mt. Pinatubo resulted in a change in ozone (Stenchikov et al., 2002; Randel et al., 1995; Brasseur and Granier, 1992) that, in turn, impacted the heating. While our experiment does not explicitly include volcanic aerosols or emissions, the prescribed ozone fields used are based on observations and thus reflect the stratospheric chemical perturbations that followed the eruption.

Analysis of the DJF mean zonal-mean ozone difference shows an increase in subtropical ozone (100–1 hPa) from 1992 to 2000, along with a decrease in tropical ozone from 10–1 hPa (Fig. 8). In contrast, from 2000 to 2020, a decrease in ozone over the subtropics (100–1 hPa) and an increase over the tropics from 10–1 hPa are observed. These changes are also consistent with the response of the radiative heating tendency (Fig. 8) in the tropics. The difference between the P2000 and P1992 years shows an increase in the tropical-to-subtropical radiative heating tendency, whereas it is negative in P2020–P2000. This perturbation appears to influence planetary wave activity, as indicated by the residual circulation and Eliassen–Palm (EP) flux diagnostics (Fig. 6), and is accompanied by stronger meridional heat transport into high latitudes (Fig. 5). Together, these wave-driven processes provide a coherent mechanism by which primarily ozone-induced heating contributed to the enhanced warming of the NH polar vortex during boreal winter from 1992 to 2000.

Therefore, the anomalous ozone distribution, itself a consequence of the volcanic event, could have altered the tropical radiative heating, and this change in heating could then have triggered the dynamical response leading to increased poleward heat transport and the subsequent polar temperature increase. Our conclusions, therefore, are that the response to CO_2 and

ozone changes is robust and that the influence of decadal variability and direct influence of the volcanic emissions can be neglected.

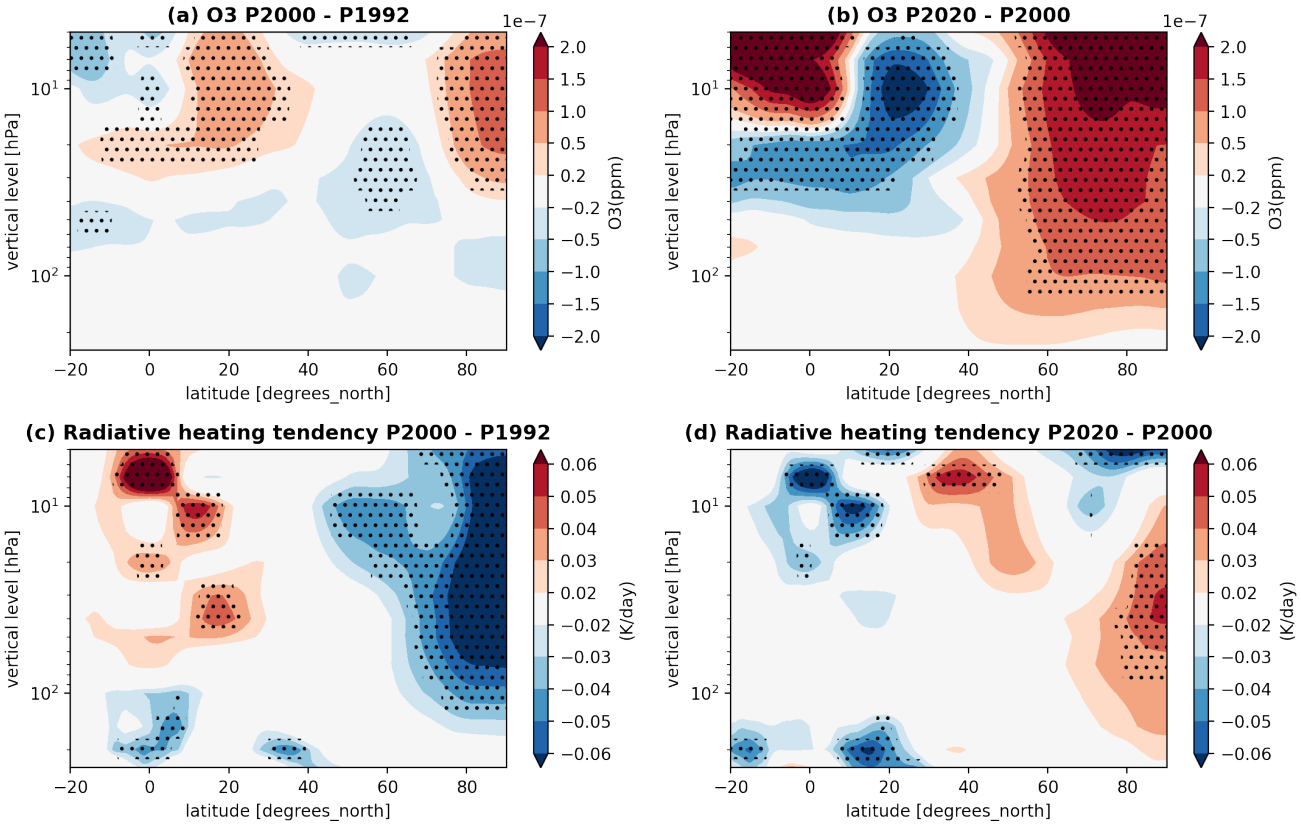

Figure 8. Zonal mean DJF (a,b) Ozone (ppm), and (c,d) radiative heating tendency (K/day) are shown for the (a,c) P2000 - P19992, and (b,d) P2020 - P2000 (95% significant differences are shown for 30-member ensemble).

Given the analysis here of the polar stratospheric response to external radiative forcing, an examination of the CMIP6 model output seems warranted. The CMIP6 multi-model mean NH DJF stratospheric temperature (65°N-90°N) shows no sign of warming from the year 1992 (Fig. 9a), and instead shows the gradual cooling that is expected based on theory. However, many CMIP models generally struggle to produce a realistic stratospheric circulation because of the low model top, insufficient vertical resolution, and inadequate aspect ratios between horizontal and vertical grids (Charlton-Perez et al., 2013; Hardiman et al., 2012; Rao and Garfinkel, 2021; Hall et al., 2021). We examined a single CMIP6 model with a well-resolved stratosphere, the NASA GISS E2 model's "Hi-Top" simulation (2-H), which is a part of the CMIP6 Historical experiment ensemble (Bauer et al., 2020; Kelley et al., 2020; Orbe et al., 2020) (Fig. 9b). Interestingly, the "Hi-Top" simulation does show a warming trend in the NH DJF stratospheric temperature in the first period (1992–2000) (7-year running mean). Given the noise from internal variability and different climate sensitivities to CO_2 and ozone forcing, the sharp warming after 1992 in the NASA

GISS E-2-2H “Hi-Top” simulation is very similar to reanalyses and to our GEOS-MITgcm simulations, although the peak warming is not perfectly aligned (Figs. 1, 9b). In contrast, the separation between the two trend regimes is not present in the “Low-Top” simulation from the NASA GISS E2-1-H historical experiment (Fig. 9b). This examination suggests that modeling the proper response of the polar stratosphere to external forcing changes requires a well-resolved stratosphere to accurately capture the heat transport. The difference in peak between GEOS-MITgcm and NASA GISS “Hi-Top" could be because the initial conditions for the ensemble simulations with GEOS-MITgcm are relatively recent in relation to the stratospheric warming period, and they may experience some advantage in the timing of the stratospheric warming relative to CMIP6 historical simulations. However, further investigation is needed.

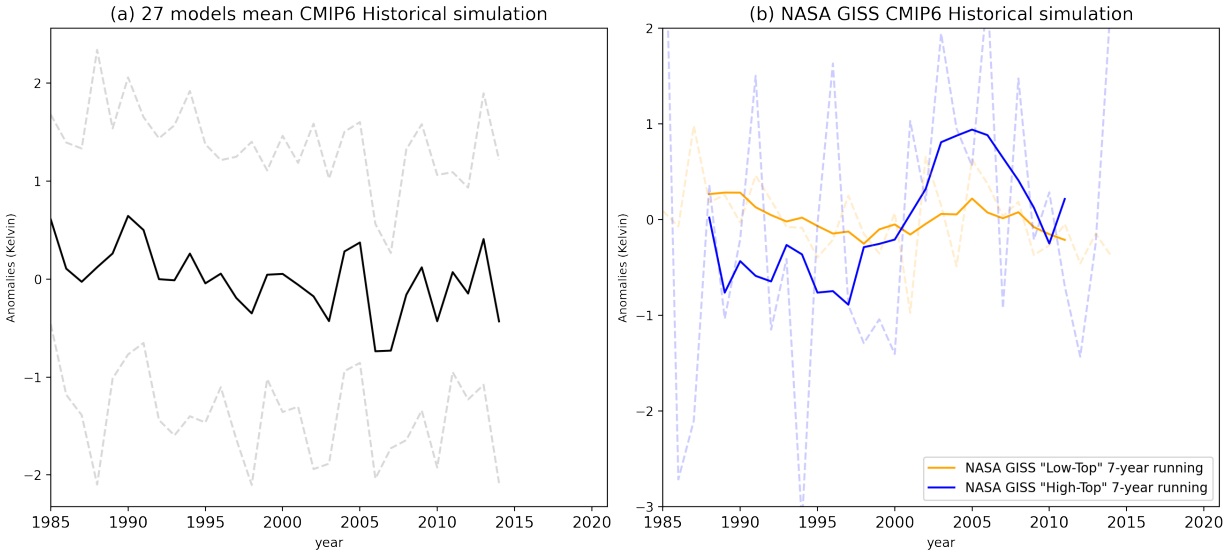

Figure 9. NH DJF mean 150 hPa-10 hPa and 65°N-90°N mean air temperature for (a) CMIP6 27 models mean Historical simulation (bold black line), and 1 std model spread are in dotted grey line. (b) shows NASA GISS "Low Top" (orange) & "High Top" (blue) simulation 7-year running mean, and actual anomalies are in dotted lines.

5 Summary

Examination of reanalyses (MERRA-2 and ERA5) shows that a cooling pattern in temperature trends has existed in the NH polar stratosphere during boreal winter from the 1980s to the 2020s (Fig. 1a), with the exception of a warming pattern from 1992 to 2000.

Our perpetual year 30-member ensemble mean GEOS-MITgcm experiments show that the NH DJF stratospheric polar temperature (65°N-90°N) response to the external forcing change (levels of CO_2 increase and ozone change) in the atmosphere exhibits a general cooling with a warming phase in 1992-2000. The difference P2000-P1992 shows a temperature increase,

whereas the temperature decreases in the P2020-P2000 (Fig. 3) difference. This opposing temperature response is in contrast with the general expectation that with increased CO_2 level in the atmosphere, the stratospheric temperature cools.

We further analyzed a 10-member ensemble mean of transient experiments from the year 1992-2020 forced with historical CO_2 levels and other observed external forcing. The results show a positive temperature trend during the year 1992-2000, and a negative temperature trend during the year 2000-2020 in the NH DJF polar stratosphere (Fig. 1a). These opposing temperature trends are consistent with the response of the perpetual experiments and reanalysis.

The longwave cooling in the NH DJF high-latitude stratosphere doesn't contribute to the local temperature response qualitatively but rather responds to it. That is, the longwave decreased (cooling increased) with temperature increase in the P2000-P1992, whereas the longwave increased (cooling decreased) with the temperature decrease in the P2020-P2000 (Fig. 4). We have shown that meridional heat transport resulting from CO_2 and ozone changes led to increased warming during the 1992–2000 period. We have argued that our experiment design excludes the influence of the low-frequency variability (e.g. ENSO, IPO, PDO, & NAO) and direct impact of the volcanic emission as a driver of the behavior seen here.

In this study we have shown a physical interpretation of the proximate cause of the NH stratospheric cooling–warming–cooling behavior. We have shown that the warming during 1992–2000 is related not to radiative effects, low-frequency modes, or direct volcanic influences, but to dynamical processes. We have traced the dynamical heating to the meridional eddy heat flux and the associated differences in wave activity. We have speculated that the change in wave activity during the warming period could be an indirect result of the Pinatubo through its influence on the ozone. We have suggested a possible indirect impact of the Pinatubo eruption, whereby the emissions from the eruption had an impact on ozone chemistry and locally increased ozone concentrations. This additional ozone generated additional tropical heating and the subsequent increase in eddy heat transport to the polar stratosphere. Studies like the one reported here are critical for the ability to predict the climate system on seasonal to decadal time scales.

Appendix A

The time-mean zonal mean meridional heat transport can be decomposed into zonal mean and zonal asymmetric components as (following Peixóto and Oort (1984), eqn 4.9):

$$[\overline{VT}] = [\overline{V}][\overline{T}] + [\overline{V^*}\,\overline{T^*}] + [\overline{V'T'}] \tag{A1}$$

Where [ ] shows the zonal mean and $*$ shows the zonal deviation of a variable. Here, $[\overline{V}][\overline{T}]$ represents the contributions of flux by steady symmetric circulations, $[\overline{V^*}\,\overline{T^*}]$ represents flux contribution by stationary eddies, and $[\overline{V'T'}]$ represents contribution of co-variance of meridional wind anomaly and temperature anomaly (transient eddies) to the meridional heat transport.

The TEM residual mass stream function, Ψ^* is calculated as follows (Andrews et al., 1987; Birner and Bönisch, 2011)

$$\Psi^* = \Psi - ag^{-1}\cos\phi\frac{[v^*\theta^*]}{\partial_p[\theta]}, \tag{A2}$$

where

$$\Psi = ag^{-1}\cos\phi\int_0^p [v]dp' \tag{A3}$$

The Eliassen Palm (EP) flux is defined as (Edmon Jr et al., 1980) :

$$\{F_\phi, F_p\} = \{-acos\phi[u^*v^*], facos\phi([v^*\theta^*]/[\theta_p]\} \tag{A4}$$

Where, ϕ is latitude and p is pressure, a is the radius of the Earth, f is the Coriolis parameter, θ is potential temperature, u is zonal wind, and v is the meridional wind.

Author contributions. A.F., A.M., D.M., A.T., E.S. and P.H. contributed to the experimental design and analysis of this study. A.F. carried out simulations. K.W. and L.C. contributed to the writing and analysis of results. All authors contributed to the ideas, analysis, and writing of the manuscript.

Competing interests. Authors have no competing interests as defined by Springer, or other interests that might be perceived to influence the results and/or discussion reported in this paper. All of the material is owned by the authors and/or no permissions are required. No conflict of interests.

Acknowledgements. DM carried out research at the Jet Propulsion Laboratory, California Institute of Technology, under contract with NASA. We would like to thank Clara Orbe (NASA GISS, NY, USA) for contributing to the initial discussion of the manuscript. High-end computing resources were provided by the NASA Center for Climate Simulate (NCCS) and the NASA Advanced Supercomputing (NAS) Division of the Ames Research Center.

References

Abalos, M., Polvani, L., Calvo, N., Kinnison, D., Ploeger, F., Randel, W., and Solomon, S.: New insights on the impact of ozone-depleting substances on the Brewer-Dobson circulation, Journal of Geophysical Research: Atmospheres, 124, 2435–2451, 2019.

Abalos, M., Calvo, N., Benito-Barca, S., Garny, H., Hardiman, S. C., Lin, P., Andrews, M. B., Butchart, N., Garcia, R., Orbe, C., et al.: The Brewer–Dobson circulation in CMIP6, Atmospheric Chemistry and Physics, 21, 13 571–13 591, 2021.

Adcroft, A. and Campin, J.-M.: Rescaled height coordinates for accurate representation of free-surface flows in ocean circulation models, Ocean Modelling, 7, 269 – 284, https://doi.org/http://doi.org/10.1016/j.ocemod.2003.09.003, 2004.

Alexander, M. A., Bhatt, U. S., Walsh, J. E., Timlin, M. S., Miller, J. S., and Scott, J. D.: The atmospheric response to realistic Arctic sea ice anomalies in an AGCM during winter, Journal of climate, 17, 890–905, 2004.

Andrews, D. G., Holton, J. R., and Leovy, C. B.: Middle atmosphere dynamics, 40, Academic press, 1987.

Austin, J., Shindell, D., Beagley, S. R., Brühl, C., Dameris, M., Manzini, E., Nagashima, T., Newman, P., Pawson, S., Pitari, G., et al.: Uncertainties and assessments of chemistry-climate models of the stratosphere, Atmospheric Chemistry and Physics, 3, 1–27, https://doi.org/10.5194/acp-3-1-2003, 2003.

Barahona, D., Molod, A., Bacmeister, J., Nenes, A., Gettelman, A., Morrison, H., Phillips, V., and Eichmann, A.: Development of two-moment cloud microphysics for liquid and ice within the NASA Goddard Earth Observing System Model (GEOS-5), Geosc. Model Dev., 7, 1733–1766, https://doi.org/10.5194/gmd-7-1733-2014, 2014.

Bauer, S. E., Tsigaridis, K., Faluvegi, G., Kelley, M., Lo, K. K., Miller, R. L., Nazarenko, L., Schmidt, G. A., and Wu, J.: Historical (1850–2014) aerosol evolution and role on climate forcing using the GISS ModelE2. 1 contribution to CMIP6, Journal of Advances in Modeling Earth Systems, 12, e2019MS001 978, https://doi.org/10.1029/2019MS001978, 2020.

Birner, T. and Bönisch, H.: Residual circulation trajectories and transit times into the extratropical lowermost stratosphere, Atmospheric Chemistry and Physics, 11, 817–827, 2011.

Bönisch, H., Engel, A., Birner, T., Hoor, P., Tarasick, D. W., and Ray, E. A.: On the structural changes in the Brewer-Dobson circulation after 2000, Atmospheric Chemistry and Physics, 11, 3937–3948, 2011.

Bosilovich, M. G.: MERRA-2: Initial evaluation of the climate, National Aeronautics and Space Administration, Goddard Space Flight Center, 2015.

Brasseur, G. and Granier, C.: Mount Pinatubo aerosols, chlorofluorocarbons, and ozone depletion, Science, 257, 1239–1242, 1992.

Butchart, N.: The Brewer-Dobson circulation, Reviews of geophysics, 52, 157–184, 2014.

Charlton-Perez, A. J., Baldwin, M. P., Birner, T., Black, R. X., Butler, A. H., Calvo, N., Davis, N. A., Gerber, E. P., Gillett, N., Hardiman, S., et al.: On the lack of stratospheric dynamical variability in low-top versions of the CMIP5 models, Journal of Geophysical Research: Atmospheres, 118, 2494–2505, https://doi.org/10.1002/jgrd.50125, 2013.

Chin, M., Ginoux, P., Kinne, S., Torres, O., Holben, B. N., Duncan, B. N., Martin, R. V., Logan, J. A., Higurashi, A., and Nakajima, T.: Tropospheric Aerosol Optical Thickness from the GOCART Model and Comparisons with Satellite and Sun Photometer Measurements, Journal of the Atmospheric Sciences, 59, 461–483, https://doi.org/10.1175/1520-0469(2002)059<0461:TAOTFT>2.0.CO;2, 2002.

Cionni, I., Eyring, V., Lamarque, J.-F., Randel, W., Stevenson, D., Wu, F., Bodeker, G., Shepherd, T., Shindell, D., and Waugh, D.: Ozone database in support of CMIP5 simulations: results and corresponding radiative forcing, Atmospheric Chemistry and Physics, 11, 11 267–11 292, 2011.

Colarco, P., da Silva, A., Chin, M., and Diehl, T.: Online simulations of global aerosol distributions in the NASA GEOS-4 model and comparisons to satellite and ground-based aerosol optical depth, J. Geophys. Res. Atmos., 115, 2010.

Edmon Jr, H., Hoskins, B., and McIntyre, M.: Eliassen-Palm cross sections for the troposphere, Journal of Atmospheric Sciences, 37, 2600–2616, https://doi.org/10.1175/1520-0469(1980)037<2600:EPCSFT>2.0.CO;2, 1980.

Eyring, V., Waugh, D., Bodeker, G., Cordero, E., Akiyoshi, H., Austin, J., Beagley, S., Boville, B., Braesicke, P., Brühl, C., et al.: Multimodel projections of stratospheric ozone in the 21st century, Journal of Geophysical Research: Atmospheres, 112, https://doi.org/10.1029/2006JD008332, 2007.

Eyring, V., Bony, S., Meehl, G. A., Senior, C. A., Stevens, B., Stouffer, R. J., and Taylor, K. E.: Overview of the Coupled Model Intercomparison Project Phase 6 (CMIP6) experimental design and organization, Geoscientific Model Development, 9, 1937–1958, https://doi.org/10.5194/gmd-9-1937-2016, 2016.

Fahad, A. A., Burls, N. J., and Strasberg, Z.: How will southern hemisphere subtropical anticyclones respond to global warming? Mechanisms and seasonality in CMIP5 and CMIP6 model projections, Climate dynamics, 55, 703–718, https://doi.org/10.1007/s00382-020-05290-7, 2020.

Fels, S., Mahlman, J., Schwarzkopf, M., and Sinclair, R.: Stratospheric sensitivity to perturbations in ozone and carbon dioxide- Radiative and dynamical response, Journal of the Atmospheric Sciences, 37, 2265–2297, 1980.

Forget, G., Campin, J.-M., Heimbach, P., Hill, C. N., Ponte, R. M., and Wunsch, C.: ECCO version 4: an integrated framework for non-linear inverse modeling and global ocean state estimation, Geoscientific Model Development, 8, 3071–3104, https://doi.org/10.5194/gmd-8-3071-2015, 2015.

Fu, Q., Solomon, S., Pahlavan, H. A., and Lin, P.: Observed changes in Brewer–Dobson circulation for 1980–2018, Environmental Research Letters, 14, 114 026, 2019.

Fujiwara, M., Manney, G. L., Gray, L. J., and Wright, J. S.: SPARC Reanalysis Intercomparison Project (S-RIP) Final Report, Tech. rep., SPARC, https://doi.org/10.17874/800dee57d13, 2022.

Garfinkel, C. I., Aquila, V., Waugh, D. W., and Oman, L. D.: Time-varying changes in the simulated structure of the Brewer–Dobson Circulation, Atmospheric Chemistry and Physics, 17, 1313–1327, 2017.

Gelaro, R., McCarty, W., Suárez, M. J., Todling, R., Molod, A., Takacs, L., Randles, C. A., Darmenov, A., Bosilovich, M. G., Reichle, R., Wargan, K., Coy, L., Cullather, R., Draper, C., Akella, S., Buchard, V., Conaty, A., da Silva, A. M., Gu, W., Kim, G.-K., Koster, R., Lucchesi, R., Merkova, D., Nielsen, J. E., Partyka, G., Pawson, S., Putman, W., Rienecker, M., Schubert, S. D., Sienkiewicz, M., and Zhao, B.: The Modern-Era Retrospective Analysis for Research and Applications, Version 2 (MERRA-2), Journal of Climate, 30, 5419–5454, https://doi.org/10.1175/JCLI-D-16-0758.1, 2017.

Gillett, N., Allen, M., and Williams, K.: Modelling the atmospheric response to doubled CO2 and depleted stratospheric ozone using a stratosphere-resolving coupled GCM, Quarterly Journal of the Royal Meteorological Society: A journal of the atmospheric sciences, applied meteorology and physical oceanography, 129, 947–966, https://doi.org/10.1256/qj.02.102, 2003.

GMAO, G. M. . A. O.: MERRA-2 instM_3d_ana_Np: 3d, Monthly mean, Instantaneous, Pressure-Level, Analysis, Analyzed Meteorological Fields V5. 12.4, NASA Goddard Earth Sciences Data and Information Services Center (DAAC) data set, p. V92O8XZ30XBI, 2015.

Hall, R. J., Mitchell, D. M., Seviour, W. J., and Wright, C. J.: Persistent model biases in the CMIP6 representation of stratospheric polar vortex variability, Journal of Geophysical Research: Atmospheres, 126, e2021JD034 759, https://doi.org/10.1029/2021JD034759, 2021.

Hardiman, S., Butchart, N., Hinton, T., Osprey, S., and Gray, L.: The effect of a well-resolved stratosphere on surface climate: Differences between CMIP5 simulations with high and low top versions of the Met Office climate model, Journal of Climate, 25, 7083–7099, https://doi.org/10.1175/JCLI-D-11-00579.1, 2012.

Hersbach, H., Bell, B., Berrisford, P., Hirahara, S., Horányi, A., Muñoz-Sabater, J., Nicolas, J., Peubey, C., Radu, R., Schepers, D., et al.: The ERA5 global reanalysis, Quarterly Journal of the Royal Meteorological Society, 146, 1999–2049, https://doi.org/10.1002/qj.3803, 2020.

Holton, J. R. and Hakim, G. J.: An introduction to dynamic meteorology: Fifth edition, Academic Press, ISBN 9780123848666, https://doi.org/10.1016/C2009-0-63394-8, 2012.

Keenlyside, N. S., Latif, M., Jungclaus, J., Kornblueh, L., and Roeckner, E.: Advancing decadal-scale climate prediction in the North Atlantic sector, Nature, 453, 84–88, https://doi.org/10.1038/nature06921, 2008.

Kelley, M., Schmidt, G. A., Nazarenko, L. S., Bauer, S. E., Ruedy, R., Russell, G. L., Ackerman, A. S., Aleinov, I., Bauer, M., Bleck, R., et al.: GISS-E2. 1: Configurations and climatology, Journal of Advances in Modeling Earth Systems, 12, e2019MS002 025, https://doi.org/10.1029/2019MS002025, 2020.

Kirtman, B., Power, S. B., Adedoyin, A. J., Boer, G. J., Bojariu, R., Camilloni, I., Doblas-Reyes, F., Fiore, A. M., Kimoto, M., Meehl, G., et al.: Near-term climate change: projections and predictability, Bulletin of the American Meteorological Society, 2013.

Kolstad, E. W., Breiteig, T., and Scaife, A. A.: The association between stratospheric weak polar vortex events and cold air outbreaks in the Northern Hemisphere, Quarterly Journal of the Royal Meteorological Society, 136, 886–893, https://doi.org/10.1002/qj.620, 2010.

Koster, R. D., Suarez, M. J., Ducharne, A., Stieglitz, M., and Kumar, P.: A Catchment-based Approach to Modeling Land Surface Processes in a General Circulation Model: 1. Model Structure, Journal of Geophysical Research: Atmosphere, 105, 24 809–24 822, 2000.

Long, C. S., Fujiwara, M., Davis, S., Mitchell, D. M., and Wright, C. J.: Climatology and interannual variability of dynamic variables in multiple reanalyses evaluated by the SPARC Reanalysis Intercomparison Project (S-RIP), Atmospheric Chemistry and Physics, 17, 14 593–14 629, 2017.

Manabe, S. and Wetherald, R. T.: Thermal Equilibrium of the Atmosphere with a Given Distribution of Relative Humidity, Journal of Atmospheric Sciences, 24, 241 – 259, https://doi.org/10.1175/1520-0469(1967)024<0241:TEOTAW>2.0.CO;2, 1967.

Manzini, E., Karpechko, A. Y., Anstey, J., Baldwin, M., Black, R., Cagnazzo, C., Calvo, N., Charlton-Perez, A., Christiansen, B., Davini, P., et al.: Northern winter climate change: Assessment of uncertainty in CMIP5 projections related to stratosphere-troposphere coupling, Journal of Geophysical Research: Atmospheres, 119, 7979–7998, 2014.

Marotzke, J., Müller, W. A., Vamborg, F. S., Becker, P., Cubasch, U., Feldmann, H., Kaspar, F., Kottmeier, C., Marini, C., Polkova, I., et al.: MiKlip: a national research project on decadal climate prediction, Bulletin of the American Meteorological Society, 97, 2379–2394, 2016.

Marshall, J., Adcroft, A., Hill, C., Perelman, L., and Heisey, C.: A finite-volume, incompressible Navier Stokes model for studies of the ocean on parallel computers, Journal of Geophysical Research: Oceans, 102, 5753–5766, https://doi.org/10.1029/96JC02775, 1997.

Meehl, G. A., Goddard, L., Boer, G., Burgman, R., Branstator, G., Cassou, C., Corti, S., Danabasoglu, G., Doblas-Reyes, F., Hawkins, E., et al.: Decadal climate prediction: an update from the trenches, Bulletin of the American Meteorological Society, 95, 243–267, 2014.

Meehl, G. A., Hu, A., Santer, B. D., and Xie, S.-P.: Contribution of the Interdecadal Pacific Oscillation to twentieth-century global surface temperature trends, Nature Climate Change, 6, 1005–1008, 2016.

Molod, A., Takacs, L., Suarez, M., and Bacmeister, J.: Development of the GEOS-5 atmospheric general circulation model: Evolution from MERRA to MERRA2, Geoscientific Model Development, 8, 1339–1356, 2015.

Newman, P. A., Nash, E. R., and Rosenfield, J. E.: What controls the temperature of the Arctic stratosphere during the spring?, Journal of Geophysical Research: Atmospheres, 106, 19 999–20 010, 2001.

Norton, W.: Sensitivity of Northern Hemisphere surface climate to simulation of the stratospheric polar vortex, Geophysical research letters, 30, 2003.

Oberländer-Hayn, S., Gerber, E. P., Abalichin, J., Akiyoshi, H., Kerschbaumer, A., Kubin, A., Kunze, M., Langematz, U., Meul, S., Michou, M., et al.: Is the Brewer-Dobson circulation increasing or moving upward?, Geophysical Research Letters, 43, 1772–1779, 2016.

Orbe, C., Rind, D., Jonas, J., Nazarenko, L., Faluvegi, G., Murray, L. T., Shindell, D. T., Tsigaridis, K., Zhou, T., Kelley, M., et al.: GISS Model E2. 2: A Climate Model Optimized for the Middle Atmosphere—2. Validation of Large-Scale Transport and Evaluation of Climate Response, Journal of Geophysical Research: Atmospheres, 125, e2020JD033 151, 2020.

Peixóto, J. P. and Oort, A. H.: Physics of climate, Reviews of Modern Physics, 56, 365, 1984.

Ploeger, F. and Garny, H.: Hemispheric asymmetries in recent changes in the stratospheric circulation, Atmospheric Chemistry and Physics, 22, 5559–5576, 2022.

Pohlmann, H., Jungclaus, J. H., Köhl, A., Stammer, D., and Marotzke, J.: Initializing Decadal Climate Predictions with the GECCO Oceanic Synthesis: Effects on the North Atlantic, Journal of Climate, 22, 3926 – 3938, https://doi.org/10.1175/2009JCLI2535.1, 2009.

Polvani, L. M., Abalos, M., Garcia, R., Kinnison, D., and Randel, W. J.: Significant weakening of Brewer-Dobson circulation trends over the 21st century as a consequence of the Montreal Protocol, Geophysical Research Letters, 45, 401–409, 2018.

Portal, A., Pasquero, C., D'andrea, F., Davini, P., Hamouda, M. E., and Rivière, G.: Influence of reduced winter land–sea contrast on the midlatitude atmospheric circulation, Journal of Climate, 35, 6237–6251, 2022.

Putman, W. and Lin, S.-J.: Finite-volume transport on various cubed-sphere grids, Journal of Computational Physics, 227, 55–78, https://doi.org/10.1016/j.jcp.2007.07.022, 2007.

Ramaswamy, V., Chanin, M.-L., Angell, J., Barnett, J., Gaffen, D., Gelman, M., Keckhut, P., Koshelkov, Y., Labitzke, K., Lin, J.-J., et al.: Stratospheric temperature trends: Observations and model simulations, Reviews of Geophysics, 39, 71–122, 2001.

Randel, W. J., Wu, F., Russell III, J., Waters, J., and Froidevaux, L.: Ozone and temperature changes in the stratosphere following the eruption of Mount Pinatubo, Journal of Geophysical Research: Atmospheres, 100, 16 753–16 764, 1995.

Randel, W. J., Shine, K. P., Austin, J., Barnett, J., Claud, C., Gillett, N. P., Keckhut, P., Langematz, U., Lin, R., Long, C., et al.: An update of observed stratospheric temperature trends, Journal of Geophysical Research: Atmospheres, 114, 2009.

Randel, W. J., Smith, A. K., Wu, F., Zou, C.-Z., and Qian, H.: Stratospheric temperature trends over 1979–2015 derived from combined SSU, MLS, and SABER satellite observations, Journal of Climate, 29, 4843–4859, 2016.

Randles, C., Da Silva, A., Buchard, V., Colarco, P., Darmenov, A., Govindaraju, R., Smirnov, A., Holben, B., Ferrare, R., Hair, J., et al.: The MERRA-2 aerosol reanalysis, 1980 onward. Part I: System description and data assimilation evaluation, Journal of climate, 30, 6823–6850, 2017.

Rao, J. and Garfinkel, C. I.: CMIP5/6 models project little change in the statistical characteristics of sudden stratospheric warmings in the 21st century, Environmental Research Letters, 16, 034 024, 2021.

Rex, M., Salawitch, R., von der Gathen, P., Harris, N., Chipperfield, M., and Naujokat, B.: Arctic ozone loss and climate change, Geophysical research letters, 31, 2004.

Rieder, H. E. and Polvani, L. M.: Are recent Arctic ozone losses caused by increasing greenhouse gases?, Geophysical Research Letters, 40, 4437–4441, 2013.

Rieder, H. E., Polvani, L. M., and Solomon, S.: Distinguishing the impacts of ozone-depleting substances and well-mixed greenhouse gases on Arctic stratospheric ozone and temperature trends, Geophysical Research Letters, 41, 2652–2660, 2014.

Rind, D., Balachandran, N., and Suozzo, R.: Climate change and the middle atmosphere. Part II: The impact of volcanic aerosols, Journal of climate, 5, 189–208, 1992.

Rind, D., Shindell, D., Lonergan, P., and Balachandran, N.: Climate change and the middle atmosphere. Part III: The doubled CO 2 climate revisited, Journal of Climate, 11, 876–894, 1998.

Santer, B. D., Po-Chedley, S., Zhao, L., Zou, C.-Z., Fu, Q., Solomon, S., Thompson, D. W., Mears, C., and Taylor, K. E.: Exceptional stratospheric contribution to human fingerprints on atmospheric temperature, Proceedings of the National Academy of Sciences, 120, e2300758 120, 2023.

Seidel, D. J., Li, J., Mears, C., Moradi, I., Nash, J., Randel, W. J., Saunders, R., Thompson, D. W., and Zou, C.-Z.: Stratospheric temperature changes during the satellite era, Journal of Geophysical Research: Atmospheres, 121, 664–681, 2016.

Shaw, T. A. and Perlwitz, J.: On the control of the residual circulation and stratospheric temperatures in the Arctic by planetary wave coupling, Journal of the Atmospheric Sciences, 71, 195–206, 2014.

Smith, D. M., Cusack, S., Colman, A. W., Folland, C. K., Harris, G. R., and Murphy, J. M.: Improved Surface Temperature Prediction for the Coming Decade from a Global Climate Model, Science, 317, 796–799, https://doi.org/10.1126/science.1139540, 2007.

Stenchikov, G., Robock, A., Ramaswamy, V., Schwarzkopf, M. D., Hamilton, K., and Ramachandran, S.: Arctic Oscillation response to the 1991 Mount Pinatubo eruption: Effects of volcanic aerosols and ozone depletion, Journal of Geophysical Research: Atmospheres, 107, ACL–28, 2002.

Stiller, G., Von Clarmann, T., Haenel, F., Funke, B., Glatthor, N., Grabowski, U., Kellmann, S., Kiefer, M., Linden, A., Lossow, S., et al.: Observed temporal evolution of global mean age of stratospheric air for the 2002 to 2010 period, Atmospheric Chemistry and Physics, 12, 3311–3331, 2012.

Stiller, G. P., Fierli, F., Ploeger, F., Cagnazzo, C., Funke, B., Haenel, F. J., Reddmann, T., Riese, M., and von Clarmann, T.: Shift of subtropical transport barriers explains observed hemispheric asymmetry of decadal trends of age of air, Atmospheric Chemistry and Physics, 17, 11 177–11 192, 2017.

Strobach, E., Molod, A., Barahona, D., Trayanov, A., Menemenlis, D., and Forget, G.: Earth system model parameter adjustment using a Green's functions approach, Geoscientific Model Development, 15, 2309–2324, 2022.

Thompson, D. W., Baldwin, M. P., and Wallace, J. M.: Stratospheric connection to Northern Hemisphere wintertime weather: Implications for prediction, Journal of Climate, 15, 1421–1428, 2002.

von der Gathen, P., Kivi, R., Wohltmann, I., Salawitch, R. J., and Rex, M.: Climate change favours large seasonal loss of Arctic ozone, Nature Communications, 12, 1–17, 2021.

Waugh, D. W., Sobel, A. H., and Polvani, L. M.: What is the polar vortex and how does it influence weather?, Bulletin of the American Meteorological Society, 98, 37–44, 2017.

Wunsch, C. and Heimbach, P.: Practical global oceanic state estimation, Physica D: Nonlinear Phenomena, 230, 197–208, 2007.

Zhou, T., DallaSanta, K. J., Orbe, C., Rind, D. H., Jonas, J. A., Nazarenko, L., Schmidt, G. A., and Russell, G.: Exploring the ENSO modulation of the QBO periods with GISS E2. 2 models, Atmospheric Chemistry and Physics, 24, 509–532, 2024.

Zhou, X., Chen, Q., Xie, F., Li, J., Li, M., Ding, R., Li, Y., Xia, X., and Cheng, Z.: Nonlinear response of Northern Hemisphere stratospheric polar vortex to the Indo–Pacific warm pool (IPWP) Niño, Scientific Reports, 9, 1–12, 2019.

Table S 11. CMIP6 Model List

Model Name	Model Name	Model Name
1 AWI-CM-1-1-MR	10 EC-Earth3-Veg	19 CESM2-FV2
2 BCC-CSM2-MR	11 IPSL-CM6A-LR	20 CESM2-WACCM
3 BCC-ESM1	12 MIROC-ES2L	21 CESM2-WACCM-FV2
4 CAMS-CSM1-0	13 MIROC6	22 NorESM2-LM
5 FGOALS-g3	14 HadGEM3-GC31-LL	23 GFDL-CM4
6 CanESM5	15 UKESM1-0-LL	24 GFDL-ESM4
7 CNRM-CM6-1	16 MRI-ESM2-0	25 NESM3
8 CNRM-ESM2-1	17 GISS-E2-1-G	26 SAM0-UNICON
9 E3SM-1-0	18 GISS-E2-1-H	27 MCM-UA-1-0

Supplementary information

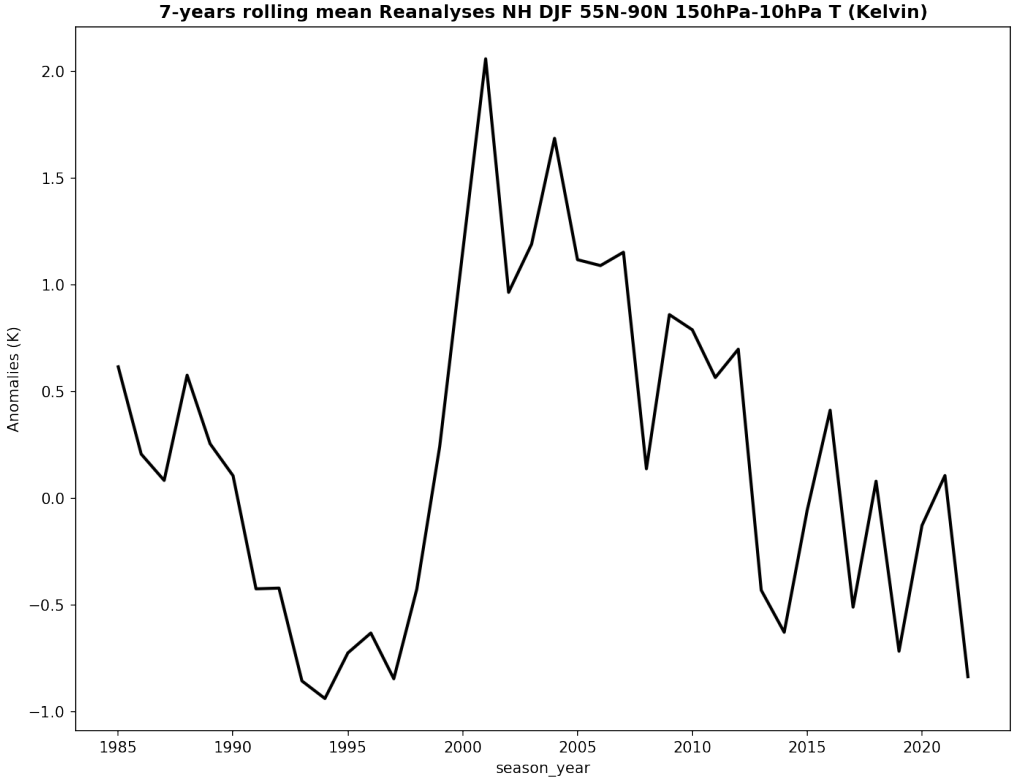

Figure S1. Rolling mean T from reanalysis

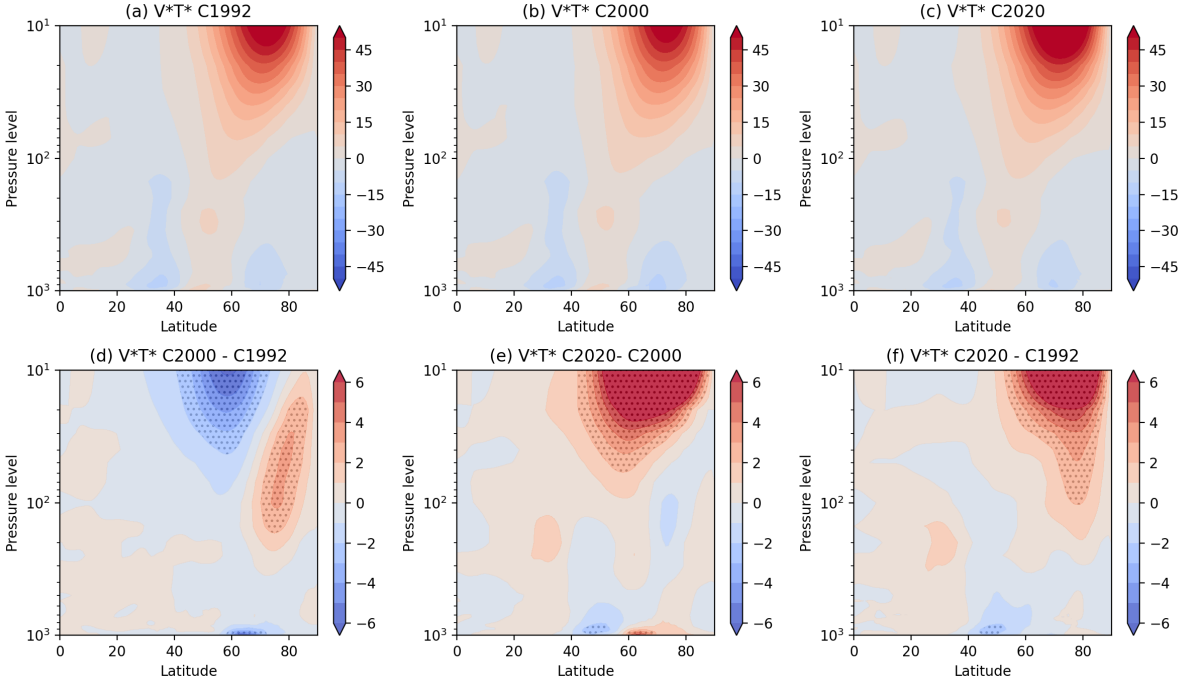

Figure S2. Zonal Mean NH DJF V^*T^* mean for (a) P1992, (b) P2000, (c) P2020, and (d) difference between P2000 - P1992, (e) difference between P2020 - P2000, (f) difference between P2020 - P1992. Figures are stippled at 95% significance computed using a difference of means 2-sided t-test from 30-member ensemble sample.

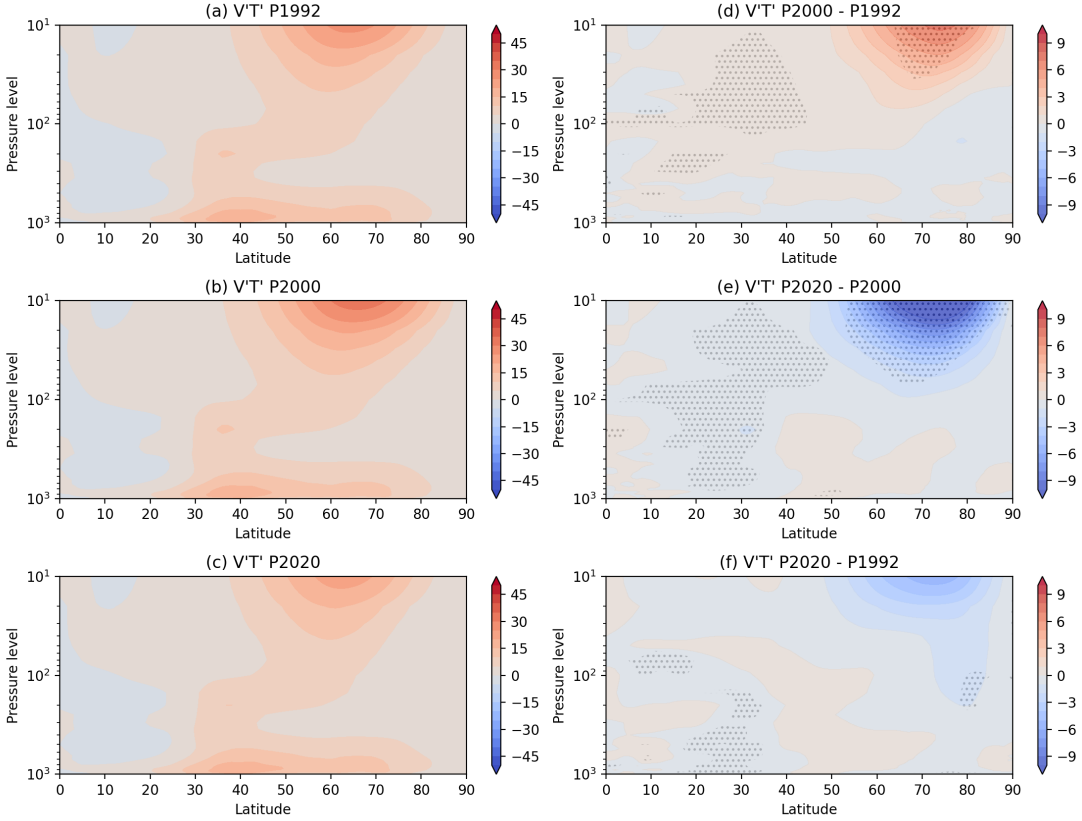

Figure S3. Zonal Mean NH DJF V'T' mean for (a) P1992, (b) P2000, (c) P2020, and (d) difference between P2000 - P1992, (e) difference between P2020 - P2000, (f) difference between P2020 - P1992. Figures are stippled at 95% significance computed using a difference of means 2-sided t-test from 30-member ensemble sample.

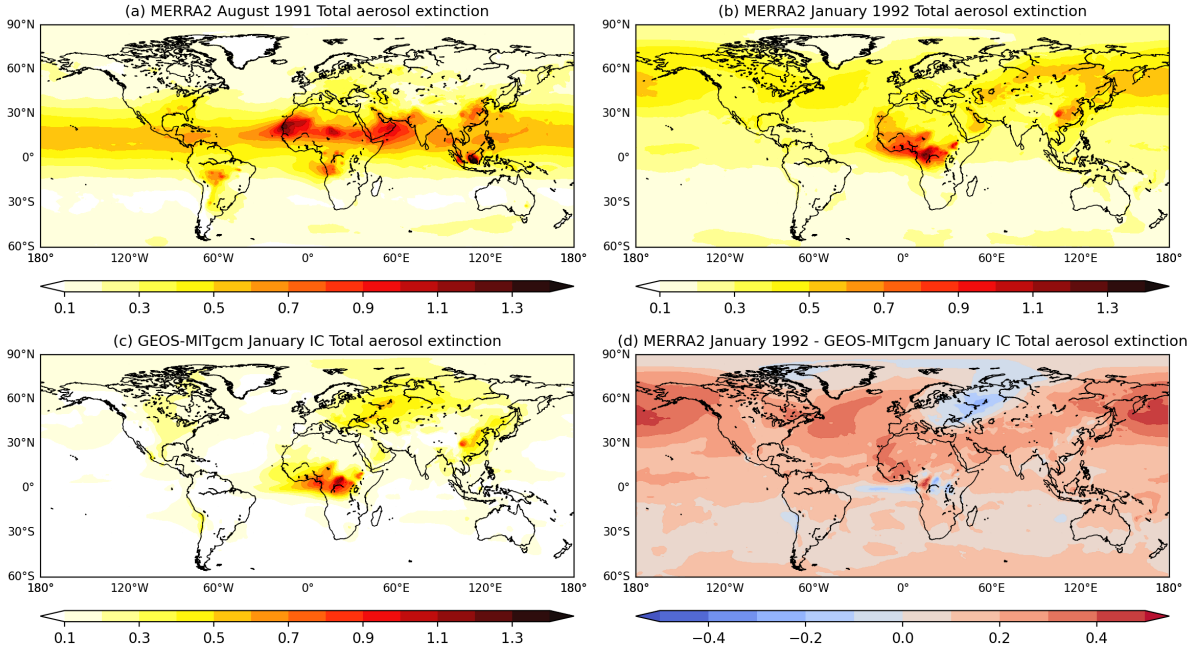

Figure S4. Total monthly mean aerosol extinction Aerosol Optical Depth [550 nm] for (a) MERRA2 August 1991, (b) MERRA2 January 1992, (c) GEOS-MITgcm January initial condition, which is used or more spun-up from this initial condition was used to initialize all experiments, and (d) MERRA2 January 1992 - GEOS-MITgcm January initial condition. The volcanic aerosol from Mount Pinatubo is visible in the MERRA2 August 1991 aerosol extinction in plot (a) (15°N, 120°E). The GEOS-MITgcm January initial condition is significantly different from observed state compared to the MERRA2 shown in plot (d), where any volcanic aerosol is not present.